Intracranial Dual-Mode IVUS and Hyperthermia Using Circular Arrays: Preliminary Experiments

Vivek Patel[1], **Edward Light**[1], **Carl Herickhoff**[1], **Gerald Grant**[1], **Gavin Britz**[1], **Christy Wilson**[1], **Mark Palmeri**[1], and **Stephen Smith**[1]

[1]Duke University, Durham, NC, USA

Abstract

In this study, we investigated the feasibility of using 3.5-Fr (3 Fr = 1 mm) circular phased-array intravascular ultrasound (IVUS) catheters for minimally invasive, image-guided hyperthermia treatment of tumors in the brain. Feasibility was demonstrated in two ways: (1) by inserting a 3.5-Fr IVUS catheter through skull burr holes, for 20 MHz brain imaging in the pig model, and (2) by testing a modified circular array for therapy potential with 18.5-MHz and 9-MHz continuous wave (CW) excitation. The imaging transducer's performance was superior to our previous 9-MHz mechanical IVUS prototype. The therapy catheter transducer was driven by CW electrical power at 18.5 MHz, achieving temperature changes reaching +8°C at a depth of 2 mm in a human glioblastoma grown on the flank of a mouse with minimal transducer resistive heating of +2°C. Further hyperthermia trials showed that 9-MHz CW excitation produced temperature changes of +4.5°C at a depth of 12 mm—a sufficient temperature rise for our long-term goal of targeted, controlled drug release via thermosensitive liposomes for therapeutic treatment of 1-cm-diameter glioblastomas.

Keywords

IVUS; hyperthermia; therapy; dual mode

Introduction

Primary malignant brain and central nervous system (CNS) tumors represent one of the most devastating forms of illness. More than 22,000 new cases and an estimated 13,100 deaths were reported in 2010 due to primary malignant brain and CNS tumors in the United States.[1] Malignant gliomas account for more than 80% of the reported cases, with 50% belonging to the most common intracranial neoplasm glioblastoma multiforme (GBM) subtype, a tumor class used in this study.[2]

Conventional therapy for malignant gliomas primarily consists of surgery, radiotherapy, and chemotherapy. Although surgery provides accurate histological diagnosis with a reduction in mass effect, the median survival with this regimen is 9 months with only 7.5% of patients surviving for 2 years.[3] Radiotherapy treatments have increased the median survival rate for patients diagnosed with malignant gliomas, but have acute side effects associated with the radiation-induced DNA damage lasting from 4 to 6 weeks after treatment.[4–8] Systemic

chemotherapy administered by mouth or intravenously may also be considered in the treatment of malignant gliomas.[9,10] The major challenge with this approach, however, is achieving a high enough concentration within the tumor bed for effective chemotherapeutic application, as there is a significant blood-brain barrier.[11] Treatment is also severely limited by the potential for systemic toxicity.

Because of the complications and challenges associated with conventional therapies, research efforts have been directed to discover novel mechanisms for drug delivery. Recent studies have illuminated the use of a thermosensitive capsule known as a liposome for effective localized chemotherapeutic treatment with a reduction in acute side effects.[12,13] Liposomes are membrane-enclosed vesicles consisting of a lipid bilayer shell surrounding an aqueous core, which can trap hydrophobic drugs and effectively encapsulate hydrophilic drugs.[14] These liposomes can be readily conjugated to a variety of adhesion ligands and antibodies for active targeting of the tumor site.[15] Rapid release of drugs from liposome capsules requires a nominal temperature increase of 4°C above the standard human body temperature—an increase that may be achieved with the use of ultrasound. Collectively, the liposome administration in conjunction with heat created via ultrasound can provide a targeted, controlled drug release in the brain vasculature providing sufficient drug concentrations within the tumor bed, increasing overall chemotherapeutic efficacy.[16]

Imaging through smaller blood vessels has become feasible with the introduction of intravascular ultrasound (IVUS) imaging.[17–19] Circular phased-array IVUS catheters typically operate at high frequencies of 20 MHz and have piezoelectric crystals contained within a sheath less than 4 Fr to effectively navigate coronary arteries with diameters ranging from 2 to 3 mm.[20] Commercially available IVUS catheters have an appropriate form factor—they are both thin and flexible, which allows for direct placement within the brain volume through an intravascular approach. As a result, they are considered here as a potential platform for intracranial ultrasound hyperthermia.[21–28]

The purpose of this project was a feasibility study of a minimally invasive, endovascular dual-mode imaging device with a long-term goal of targeted, controlled drug release via thermosensitive liposomes for the treatment of malignant brain tumors. The design goal is a thin, flexible, dual-mode imaging ultrasound catheter that can provide ultrasound hyperthermia with real-time imaging to allow for navigation through the brain vasculature. Ideally, the dual-mode transducer would be positioned adjacent to a malignant brain tumor for direct visualization followed by targeted ultrasound hyperthermia to open the blood-brain barrier and to trigger the release of chemotherapeutics from liposomes (Figure 1). Using fluoroscopic guidance, physicians could direct the catheter to a site adjacent to the malignant tumor for visualization and hyperthermia via ultrasound to activate thermosensitive liposomes that are conjugated to molecularly target sites of tumor angiogenesis.

Previously, in our laboratory, 10- and 12-Fr phased-array catheter probes were used for in vivo canine brain studies and to evaluate various aperture sizes for IVUS transducers in a thermal model.[29,30] In addition, we investigated the merit of a 9-MHz PZT-4 transducer by fabricating and testing both therapeutic and imaging prototypes by modifying commercial 3.5-Fr rotating piston IVUS catheters.[31] We achieved minimally invasive brain imaging in the sheep model (Figure 2) and more than 10°C heating of a human glioblastoma xenograft in the flank of a nude mouse. However, our 9-MHz images were not satisfactory, showing only the lateral ventricles, and it is difficult to stop the beam of a rotating IVUS catheter for the hyperthermia mode.

Because of the unsatisfactory imaging performance of our previous rotating piston IVUS prototype, we investigated the feasibility of a different approach using a circular IVUS phased array with a higher resonance frequency of 20 MHz, providing increased resolution for image-guided therapy in the brain. By modifying the same IVUS transducer to provide hyperthermia at an off-resonance spectral peak of 9 MHz, we simulated a novel dual-mode device—operating at 20 MHz for imaging and 9 MHz for heating—for intracranial therapeutic applications through preliminary studies of in vivo imaging, hyperthermia in a tissue phantom, and in vivo hyperthermia in a mouse model.

Materials and Method

Imaging Porcine Brain

To assess the imaging performance of our prototypes, unmodified Volcano Eagle Eye Gold and Platinum imaging catheters were used.[33,34] Porcine superdural imaging was performed in vivo in two pigs. The Institutional Animal Care and Use Committee at Duke University approved the procedure. A superocular burr hole was drilled along the temporal lobe region and angled anteriorly. This allowed IVUS catheter insertion in the intracranial space for superdural imaging, such that the catheter moved slightly obliquely toward the midline and the frontal lobe (Figure 3). Real-time images of the vessels were acquired with the Volcano imaging transducers using the Volcano s5 scanner.

Therapeutic Prototypes

For our prototypes, five Volcano Eagle Eye Gold imaging catheters were modified. Each transducer consists of a circular array of 64 piezoelectric elements operating at a nominal frequency of 20 MHz, attached to five ASIC chips. Ideally, software code modifications and minor hardware modifications could be used to electronically short-circuit a portion of the elements together for ultrasound hyperthermia. The modifications would allow for quick switching between an imaging phased-array mode and an electronically short-circuited hyperthermia mode for clinical applications; however, we did not have access to the Volcano scanner software. In our experimental approach to determine feasibility, we physically shorted some of the elements together and used an external waveform generator as a power source to simulate such software modifications.

Much of the original 150-cm catheter length was cut from the transducer, leaving a total length of about 10 cm. Each trace originated from one of the five flex circuit boards in groups of 13. The polyimide surface covering the transducer elements was partially removed by making a cut close to the flex board and carefully peeling back the polyimide layer. Silver paint was applied between some of the exposed traces to create a short between 16 elements (Figure 4).

Impedance analysis of the transducer before hardware modifications could not be performed due to the unknown schematic of electronics of the commercially available catheter; however, the Volcano corporation specifies a 20-MHz transducer. Figure 5a illustrates impedance results from a typical catheter transducer prototype showing a spectral peak at 18.5 MHz.

A calibrated hydrophone membrane (S4-251, Sonora Medical Systems, Longmont, Colorado, USA) was used in a water tank with a 60-V pp, three-cycle burst sine wave to assess the transmit angular beam plot of the modified transducer. The apparatus was designed so that the transducer would be positioned in the center of a circularly rotating stage that held the hydrophone. Ideally, there would be a fixed beam width ranging from 30 to 90 degrees based on the number of short-circuited elements. Figure 5b shows a −6-dB beam width of roughly 55 degrees—typical of the modified IVUS catheters. Measurements

of ISPTP (spatial peak, temporal peak intensity) were also made accompanying therapeutic exposure experiments.

Thermal Testing

To assess the therapeutic potential, both a 4-cm diameter disk of tissue-mimicking material (National Physical Laboratory, Teddington, UK, $= 0.22$ Np cm^{-1} MHz^{-1}) and a human glioblastoma tumor grown on the flank of a mouse were tested. The catheter transducer was placed about 1 mm above the tissue-mimicking phantom, and a type T, 33-gauge, hypodermic needle thermocouple (HYP-0, Omega Engineering, Stamford, Connecticut, USA) was inserted about 1.5 mm below the surface of the material and aligned with the center of the transducer transmit aperture. Another thermocouple needle was placed on the backside of the transducer to measure resistive heating (Figure 6). The small diameter, fine-wire thermocouple was chosen to reduce the effects of artifacts (viscous heating, conduction along the wire, and reflections) providing thermal measurements. A waveform generator (Model 33250, Agilent, Santa Clara, California, USA) and 25-W radio frequency (RF) power amplifier (Model 525LA, ENI, Rochester, New York, USA) were used to produce an 18.5-MHz continuous wave (CW) transmit signal. Electrical input to the therapy prototype transducer, including average forward and reflected power, was measured with a power reflection meter (NRT; Rhode & Schwarz, Munich, Germany).

Two hyperthermia trials were conducted on a human glioblastoma xenograft tumor that was grown on the flank of a nude mouse. The animal was anesthetized with 100 mg/kg ketamine/xylazine and monitored by toe-pinch reflex. The anesthetic was readministered as needed on a per animal basis when the animal responded to the toe pinch. Animal body temperature was maintained at 37°C using a homeothermic heating blanket. To simulate hyperthermia in the body, the skin was removed at the location of the tumor. A thermocouple needle was positioned 2 mm below the surface of the tissue, and the therapeutic prototype was positioned at the surface of the tumor with a minimum amount of ultrasound gel between the transducer and the tumor surface (Figure 7). CW excitation at 18.5 MHz was applied for 90-second intervals at net forward electrical power levels of 2.2 W, 1.2 W, and 900 mW with 60 seconds of off-time between each excitation to allow the tissue temperature to recover to near its baseline.

Results

Imaging Results

The 3.5 Fr Volcano Eagle Eye Gold and Platinum Catheters were used for 20-MHz imaging in the brain. Figure 8 shows two images produced during an in vivo porcine brain study. Figure 8a shows an oblique scan that includes the skull and multiple blood vessels in long axis. The Volcano ChromaFlo feature was implemented for Figure 8b, which shows a coronal view of the porcine brain with color flow in the short axis of three vessels. By comparing the images in Figure 8 and Figure 2b, we concluded that the Volcano Eagle Eye Platinum outperforms our previously constructed 9-MHz IVUS prototype[31] with more, clearly distinguished anatomical features albeit with less depth penetration. Although the imaging results are very promising for our dual-mode approach, further in vivo experiments should be conducted in porcine models with tumors to fully characterize the imaging capabilities of the 20-MHz IVUS array.

Ultrasound Hyperthermia at 18.5 MHz

The therapeutic prototype was able to achieve significant hyperthermia results in both the tissue phantom and the in vivo mouse study. A temperature rise of 8.5°C roughly 2 mm deep in the tissue phantom and a temperature rise of 2°C on the backside of the transducer were

observed while heating for 2 minutes with CW excitation at a net forward electric power level of 3.2 W with an ISPTP of 5.31 W/cm^2 (Figure 9). The minimal temperature rise of 2°C on the backside of the transducer indicates that a majority of the hyperthermia resulted from the ultrasound beam rather than resistive losses in the array.

Further hyperthermia trials were conducted on the human glioblastoma xenograft (Figure 10). In 90 seconds of CW excitation at a net forward electric power of 2.2 W, a temperature rise of 8°C was observed. Subsequent CW excitations at power levels of 1.2 W and 900 mW produced temperature rises of 4.5°C and 3°C, respectively. ISPTP values for each excitation were found to be 5.14 W/cm^2, 2.62 W/cm^2, and 1.83 W/cm^2, respectively. We note the sharper increase and immediate decrease in temperature as compared with the tissue phantom results, which may be a result of less viscous interactions in the medium and absorption due to different tissue types.

Ultrasound Hyperthermia at 9 MHz

A subsequent measurement of the transmit power spectrum with the hydrophone for the modified catheter indicated a small, off-resonance peak at about 9 MHz, which might increase the ultrasound penetration (Figure 11a). In addition, the beam pattern for the 9-MHz transducer prototype shows a wider response than the 18-MHz prototype by roughly 8 degrees (Figure 11b).

For this frequency, a temperature rise of 5.5°C was observed at a depth of 2.5 mm in tissue phantom (Figure 12a). Net forward electric power input was measured as 2.8 W with an ISPTP of 2.56 W/cm^2. There was 60 seconds of excitation followed by 60 seconds of off-time for the trial.

Because this excitation was driving the transducer off resonance, we were more concerned with resistive heating issues. In addition, the experimental setup was redesigned to measure a thermal map in the phantom. Instead of positioning the transducer above the disk, we placed the transducer at the edge of the disk in a vertical position and inserted thermocouples vertically into the phantom at a depth of 2 mm. Heating data were observed on the backside of the transducer as well as various locations both centered and off-centered from the transmit aperture of the transducer (Figure 12b). The figure shows that 9-MHz CW excitation produced temperature changes ranging from +7°C at a 2-mm depth to +4.5°C at a depth of 12 mm—both sufficient temperature increases for the therapeutic treatment of 1-cm diameter glioblastomas. Meanwhile, the temperature rise on the backside of the catheter was 3.5°C. The discrepancy from the left and right 3-mm offsets can be attributed to slight misalignments of the transducer aperture.

Discussion

Volcano Eagle Eye Gold IVUS catheters were modified to create hyperthermia prototypes for dual-mode IVUS hyperthermia applications. Physically short-circuiting the transducer elements enabled us to produce a wide acoustic beam for hyperthermia experiments. Impedance testing and power spectrum analysis of the modified transducers indicated a high-frequency spectral peak around 18.5 MHz as well as a low-frequency spectral peak at 9 Mhz. Hydrophone measurements showed that the roughly 15-element short circuit produced a −6 dB beam width of 45 to 55 degrees.

Results from the hyperthermia experiments seem promising for the therapeutic application of a dual-mode IVUS device. However, the experimental results may be skewed due to the size of the thermocouple needles used in our hyperthermia trials. The 200-μm diameter of the thermocouple needles is larger than the ultrasonic wavelengths used for heating, which

may have had an influence on the temperature rises due to viscous interactions and scattering from the thermocouple needles. Future experiments should incorporate smaller thermocouple needles for a more accurate demonstration of therapeutic efficacy as well as magnetic resonance imaging (MRI) thermometry to monitor these heating artifacts.

Data from the 9-MHz heating map suggests a study should be conducted with fluid flow around the transducer to better simulate cooling in the vasculature. Ideally, this simulation of blood flow would cool the transducer at its surface and minimize the effects of the resistive heating. Throughout the testing process, some of our therapeutic prototypes failed after several experiments, which we believe may also be a result of resistive heating. In addition, the 7°C temperature rise only 1 mm away from the transmit aperture may lead to vessel damage in the brain vasculature. Experiments with fluid flow should show reduction in the effect of resistive heating, resulting in a more uniform heating distribution at all depths as well as improved transducer life.

Ultimately, both software code modifications and hardware modifications will be required for the use of our suggested dual-mode device. Currently, the Volcano system and IVUS array are not designed to handle the high power levels of CW input required for hyperthermia. With our promising application of hyperthermia, it is likely that changes should be made to both the system electronics and transducer to handle the increased power levels.

Conclusion

We have presented both in vivo imaging and hyperthermia data that are indicative of successful dual-mode IVUS operation. The 20-MHz circular phased-array imaging catheter outperformed the previously constructed 3.5-Fr mechanical IVUS catheter more clearly distinguishing anatomical features in a porcine brain. In addition, the therapy prototype achieved a temperature rise of 8°C in a human glioblastoma at 18.5 MHz and a depth of 2 mm as well as a temperature rise of 4.5°C in a tissue phantom at 9 MHz and a depth of 12 mm—both more than the 4°C required for clinical applications of thermosensitive liposomes. Our studies indicate sufficient heating at depths required for 1-cm tumor beds. Our hardware IVUS catheter short circuits have mimicked modifications that can already be implemented in an IVUS scanner via software. In addition, this study indicates that future design of a dual-mode circular IVUS phased array should incorporate both a high-frequency imaging mode with pulsed excitation and a low-frequency hyperthermia mode with CW excitation for therapy. Ultimately, our results indicate that development of intracranial dual-mode IVUS circular arrays may be feasible.

Acknowledgments

References

1. American Cancer Society. Cancer Facts and Figures 2010. Atlanta, GA: American Cancer Society; 2009.

2. Kleihues, P.; Cavenee, WK. Pathology and Genetics of Tumours of the Nervous System. 2nd ed.. Lyon, France: IARC Press; 2000. International Agency for Research on Cancer.

3. Mareel, M.; Dierckx, R.; De Neve, W. Anti-invasive brain tumor therapy: general aspects and future strategies. In: Mikkelsen, T., editor. Brain Tumor Invasion: Biological, Clinical, and Therapeutic Considerations. New York: Wiley-Liss; 1998. p. 391-414.

4. Bernstein, MBM., editor. Neuro-Oncology: The Essentials. New York: Thieme Medical; 2000.

5. Cabantog AM, Bernstein M. Complications of First Craniotomy for Intraaxial Brain-Tumor. Can J Neurol Sci. 1994; 21(3):213–218. [PubMed: 8000976]

6. Fadul C, Wood J, Thaler H, Galicich J, Patterson RH, Posner JB. Morbidity and mortality of craniotomy for excision of supratentorial gliomas. Neurology. 1988; 38(9):1374–1379. [PubMed: 3412585]

7. Schottenfeld, DFJ. Cancer Epidemiology and Prevention. 2nd ed.. New York: Oxford University Press; 1996.

8. Mikkelsen, T.; Bjerkvig, R. Brain Tumor Invasion: Biological, Cinical, and Therapeutic Considerations. New York: Wiley-Liss; 1998.

9. Prados, MD. Systemic chemotherapy. In: Bernstein, M.; Berger, MS., editors. Neuro-Oncology: The Essentials. New York: Thieme Medical Publishers; 2000. p. 228-229.

10. Wrensch M, Bondy ML, Wiencke J, Yost M. Environmental risk-factors for primary malignant brain-tumors—a review. J Neurooncol. 1993; 17(1):47–64. [PubMed: 8120572]

11. Lesniak, MS.; Frazier, J.; Brem, H. Targeting drugs to tumors of the central nervous system. In: Ali-Osman, F., editor. Contemporary Cancer Research: Brain Tumors. Totowa, NJ: Humana Press; 2005.

12. Kheirolomoom A, Dayton PA, Lum AFH, Little E, Paoli EE, Zheng HR, et al. Acoustically-active microbubbles conjugated to liposomes: characterization of a proposed drug delivery vehicle. J Control Release. 2007; 118(3):275–284. [PubMed: 17300849]

13. Bloch SH, Dayton PA, Ferrara KW. Targeted imaging using ultrasound contrast agents. IEEE Eng Med Biol. 2004; 23(5):18–29.

14. Ponce AM, Vujaskovic Z, Yuan F, Needham D, Dewhirst MW. Hyperthermia mediated liposomal drug delivery. Int J Hyperther. 2006; 22(3):205–213.

15. Dayton PA, Ferrara KW. Targeted imaging using ultrasound. J Magn Reson Imaging. 2002; 16(4): 362–377. [PubMed: 12353252]

16. Guthkelch AN, Carter LP, Cassady JR, Hynynen KH, Iacono RP, Johnson PC, et al. Treatment of malignant brain-tumors with focused ultrasound hyperthermia and radiation—results of a phase-I trial. J Neurooncol. 1991; 10(3):271–284. [PubMed: 1654406]

17. Mehran, RMG.; Pichard, A.; Kent, K.; Satler, L.; Popma, J.; Leon, M. Clinical application of intravascular ultrasound imaging in a center with high-volume preintervention ultrasound imaging. In: Siegel, RJ., editor. Intravascular Ultrasound Imaging in Coronary Artery Disease. New York: Dekker; 1998. p. 59-75.

18. Nishioka, T.; Luo, H.; Eigler, N.; Siegel, R.; Tabak, S. Clinical application of IVUS imaging in a center with selective use of IVUS imaging. In: Siegel, RJ., editor. Intravascular Ultrasound Imaging in Coronary Artery Disease. New York: Dekker; 1998. p. 75-95.

19. Uren, NYP.; Fitzgerald, P. Prognostic implications of intravascular ultrasound imaging after coronary intervention. In: Siegel, RJ., editor. Intravascular Ultrasound Imaging in Coronary Artery Disease. New York: Dekker; 1998. p. 39-57.

20. Foster, F.; Ryan, L.; Lockwood, G. High frequency ultrasound scanning of the arterial wall. In: Roelandt, J., editor. Intravascular Ultrasound. Boston, MA: Kluwer Academic Publishers; 1993. p. 91-108.

21. Eebel, RE. Intravascular Ultrasound. St. Louis, MO: Mosby; 1998.

22. Phillips, LC.; Klibanov, AL.; Wamhoff, BR.; Hossack, JA.; Bowles, DK. Intravascular Ultrasound Mediated Delivery of DNA via Microbubble Carriers to an Injured Porcine Artery In Vivo; IEEE Ultrason Symp; 2008. p. 1-4.Appendix: 1154-7.

23. Kilroy, J.; Patil, A.; Hossack, J. Ultrasound catheter for microbubble based drug delivery; IEEE Ultrason Symp; 2009. p. 2770-2773.

24. Kruse, DE.; Stephens, DN.; Paoli, EE.; Barnes, SH.; Ferrara, KW. Spatial and temporal controlled tissue heating on a modified clinical ultrasound scanner for generating mild hyperthermia in tumors; IEEE Ultrason Symp Proceedings; 2007. p. 1-6.p. 313-318.

25. Stephens, DN.; Lu, XM.; Proulx, T.; Walters, W.; Dayton, P.; Tartis, M., et al. Multi-frequency Array Development for Drug Delivery Therapies; IEEE Ultrason Symp; 2006. p. 1-5.Proceedings: 66-9.

26. Ebbini ES, Yao H, Shrestha A. Dual-mode ultrasound phased arrays for image-guided surgery. Ultrason Imag. 2006; 28(2):65–82.

27. Makin IRS, Mast TD, Faidi W, Runk MM, Barthe PG, Slayton MH. Miniaturized ultrasound arrays for interstitial ablation and imaging. Ultrasound Med Biol. 2005; 31(11):1539–1550. [PubMed: 16286031]

28. Gentry KL, Smith SW. Integrated catheter for 3-D intracardiac echo cardiography and ultrasound ablation. IEEE Trans Ultrason Ferroelectr Freq Control. 2004; 51(7):800–808. [PubMed: 15300999]

29. Herickhoff CD, Light ED, Bing KF, Mukundan S, Grant GA, Wolf PD, et al. Dual-mode intracranial catheter integrating 3D ultrasound imaging and hyperthermia for neuro-oncology: feasibility study. Ultrason Imag. 2009; 31(2):81–100.

30. Herickhoff CD, Grant GA, Britz GW, Smith SW. Dual-mode IVUS catheter for intracranial image-guided hyperthermia: feasibility study. IEEE Trans Ultrason Ferroelectr Freq Control. 2010; 57(11):2572–2584. [PubMed: 21041144]

31. Herickhoff CD, Wilson CM, Grant GA, Britz GW, Light ED, Palmeri ML, et al. Dual-mode IVUS transducer for image-guided brain therapy: preliminary experiments. Ultrasound Med Biol. 2011; 37(10):1667–1676. [PubMed: 21856073]

32. Fletcher, T. Canine planar anatomy. 2006. Available from http://vanat.cvm.umn.edu/planar/

33. Crowe JR, Shapo BM, Stephens DN, Bleam D, Eberle MJ, Cespedes EI, et al. Blood speed imaging with an intraluminal array. IEEE Trans Ultrason Ferroelectr Freq Control. 2000; 47(3):672–681. [PubMed: 18238595]

34. Odonnell M, Eberle MJ, Stephens DN, Litzza JL, SanVicente K, Shapo BM. Synthetic phased arrays for intraluminal imaging of coronary arteries. IEEE Trans Ultrason Ferroelectr Freq Control. 1997; 44(3):714–721.
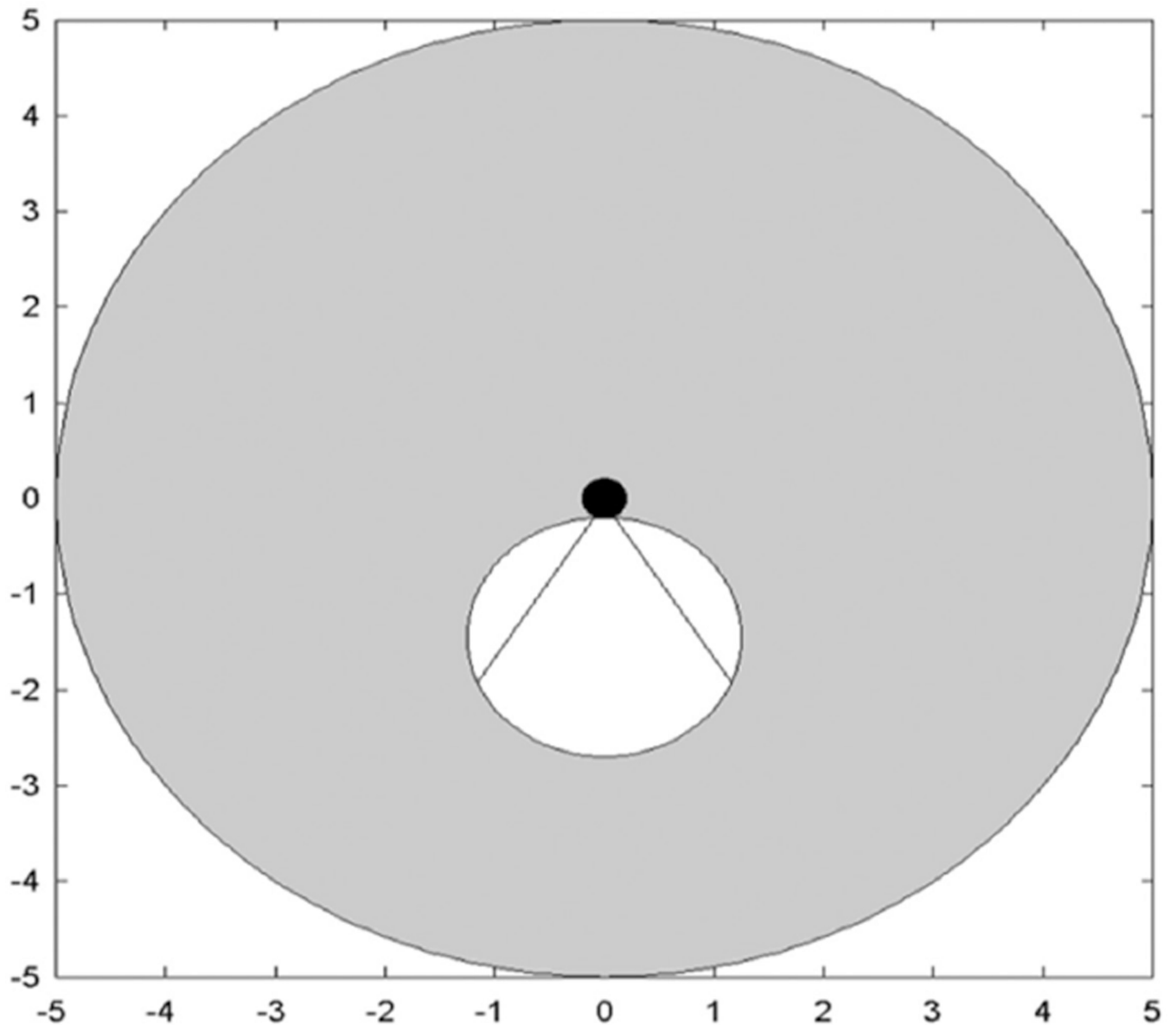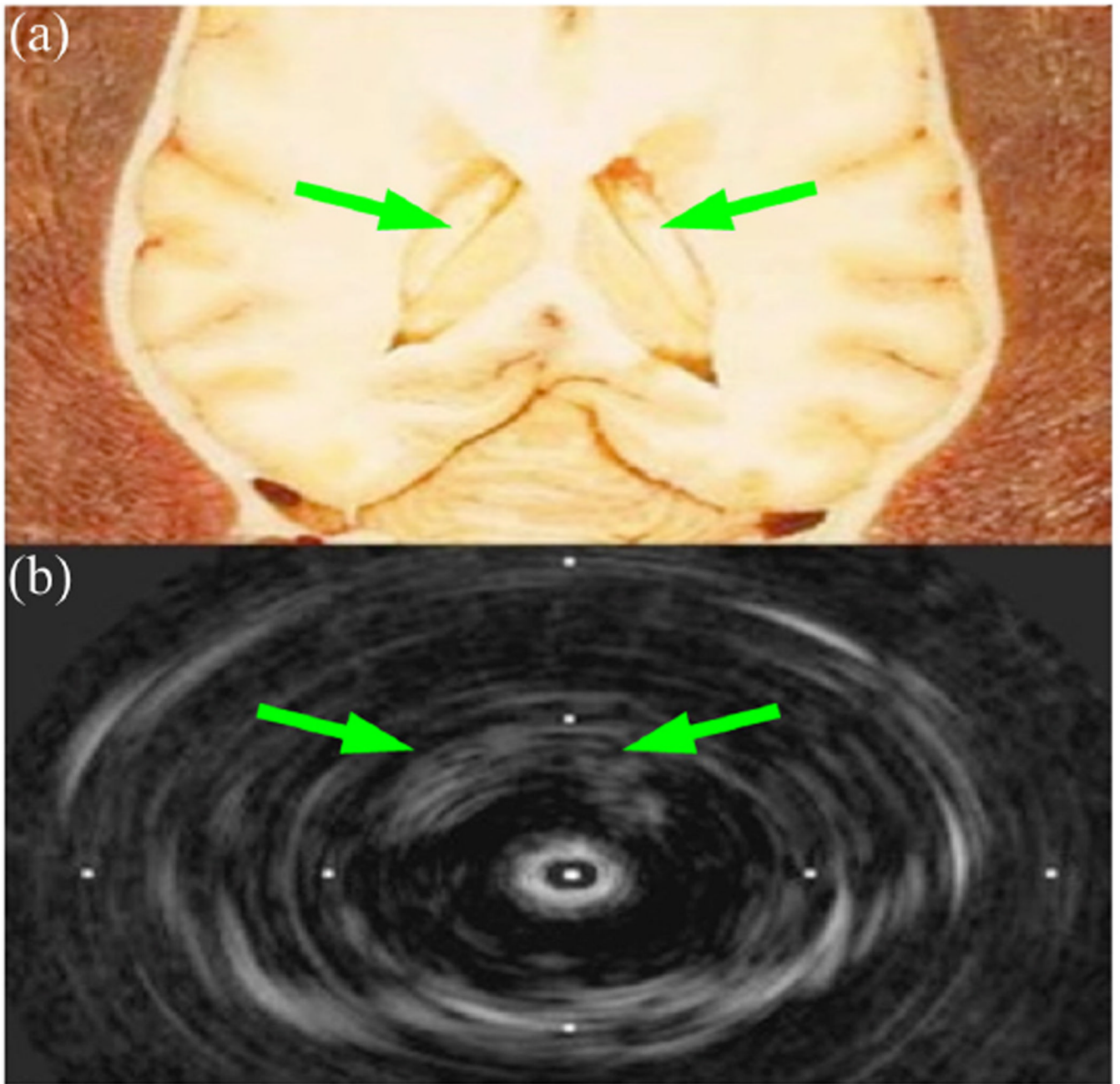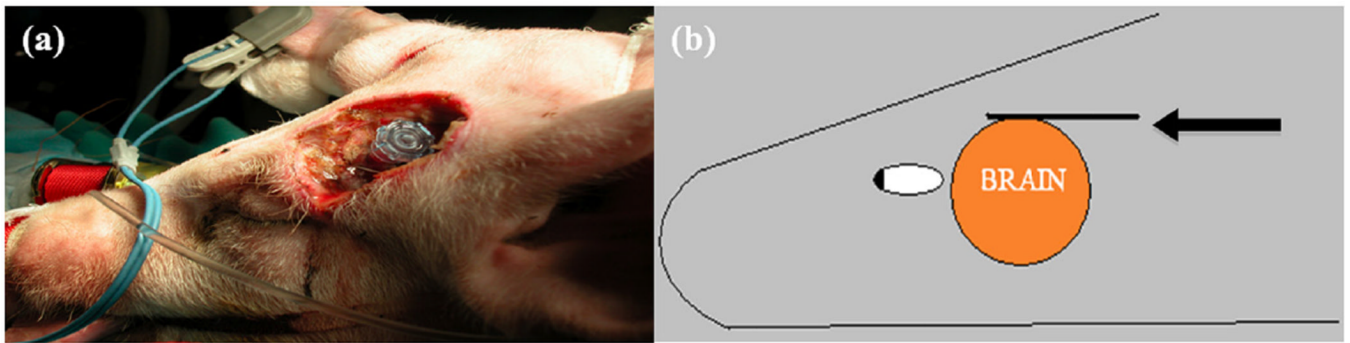
Figure 1.
Schematic of idealized dual-mode IVUS operation. Radial imaging field of view (gray) for circular phased array. White circle shows boundaries of the tumor. Hyperthermia beam (straight lines show full width at half maximum) from catheter (black) directed at tumor. Scale in centimeter.
IVUS = intravascular ultrasound.

Figure 2.
Postmortem sheep brain 9-MHz image. (a) Anatomical diagram of lateral ventricles
(arrows), with permission.[32] (b) Modified mechanical IVUS prototype image.[31] Tick marks
16-mm spacing.
IVUS = intravascular ultrasound.

Figure 3.
(a) Porcine superocular burr hole drilled along temporal lobe for oblique catheter insertion.
(b) Cross-sectional sketch of transducer placement on the dura. Arrow points to the 20-MHz IVUS transducer.
IVUS = intravascular ultrasound.
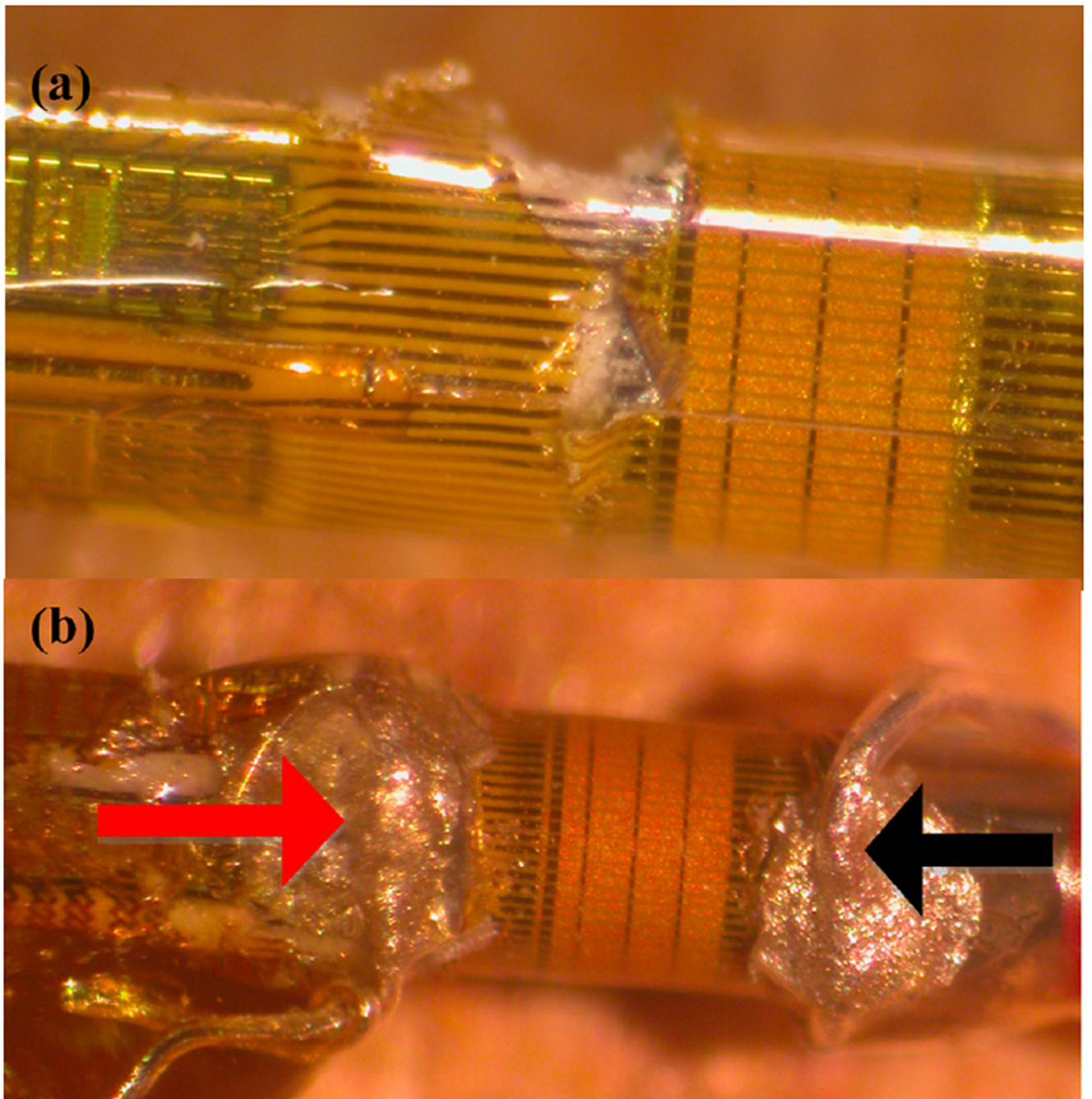
Figure 4.
(a) Original IVUS catheter with gold piezoelectric elements. Black lines extending from piezoelectric elements represent traces. Photo shows peeling of polyimide layer for establishment of hot connection. (b) Completed therapeutic prototype with hot connection (red arrow), and ground connection (black arrow).
IVUS = intravascular ultrasound.
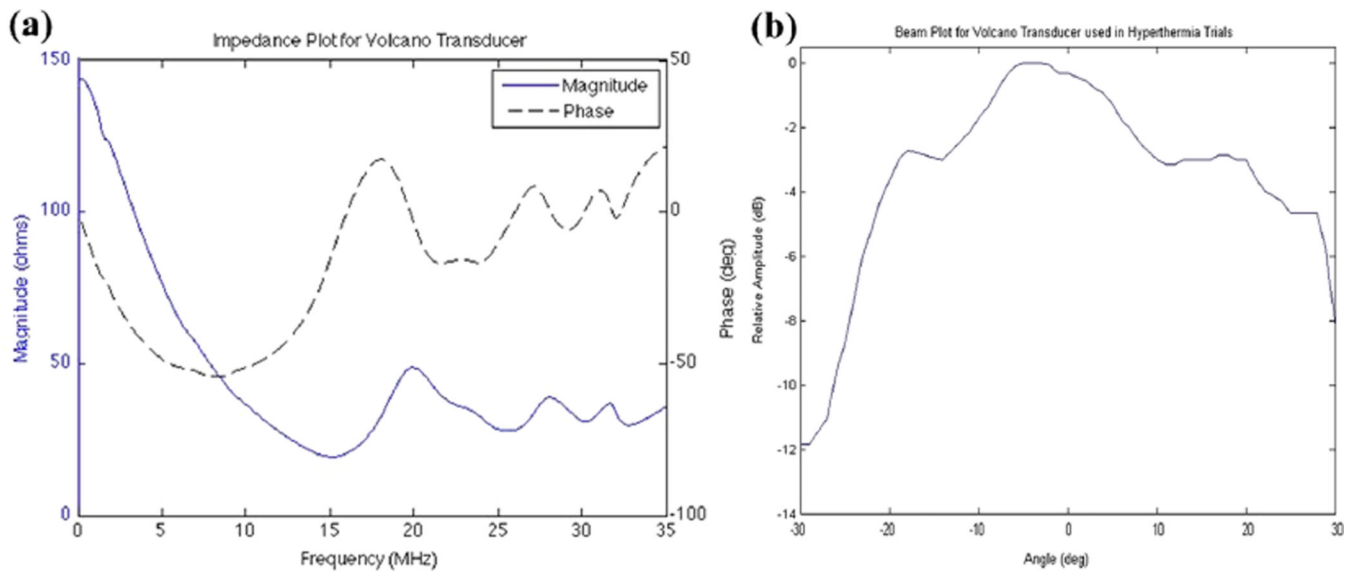
Figure 5.
(a) Impedance plot for the short-circuit prototype with large spectral peak around 18.5 MHz.
(b) Beam plot for the short-circuit prototype at 18.5 MHz with −6-dB beam width of roughly
55 degrees.

Figure 6.
Heating schematic for phantom disk. The catheter (gray) is positioned close to the surface of the tissue-mimicking phantom (yellow) with the transducer elements (red) centered on the thermocouple needle (black). Note also a thermocouple needle (black line) on the backside of the transducer elements.
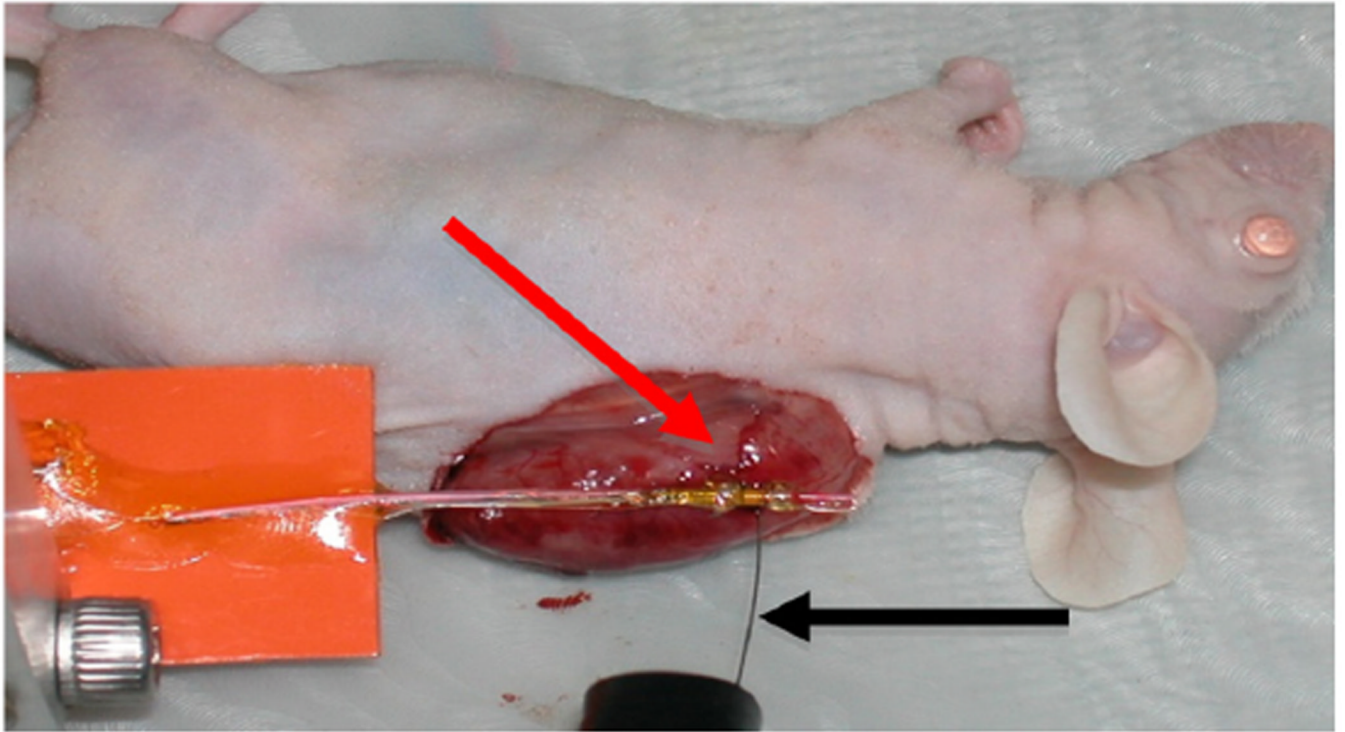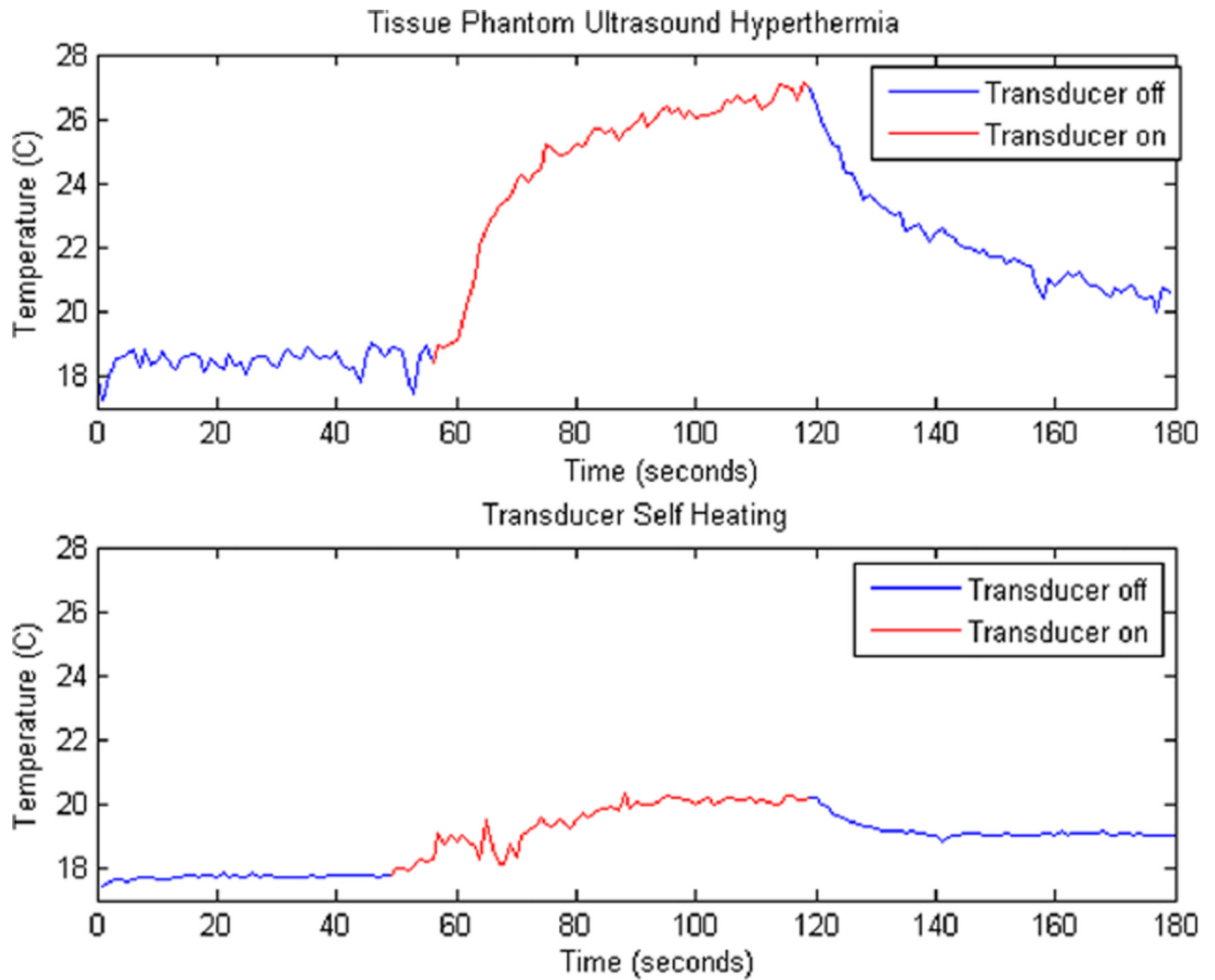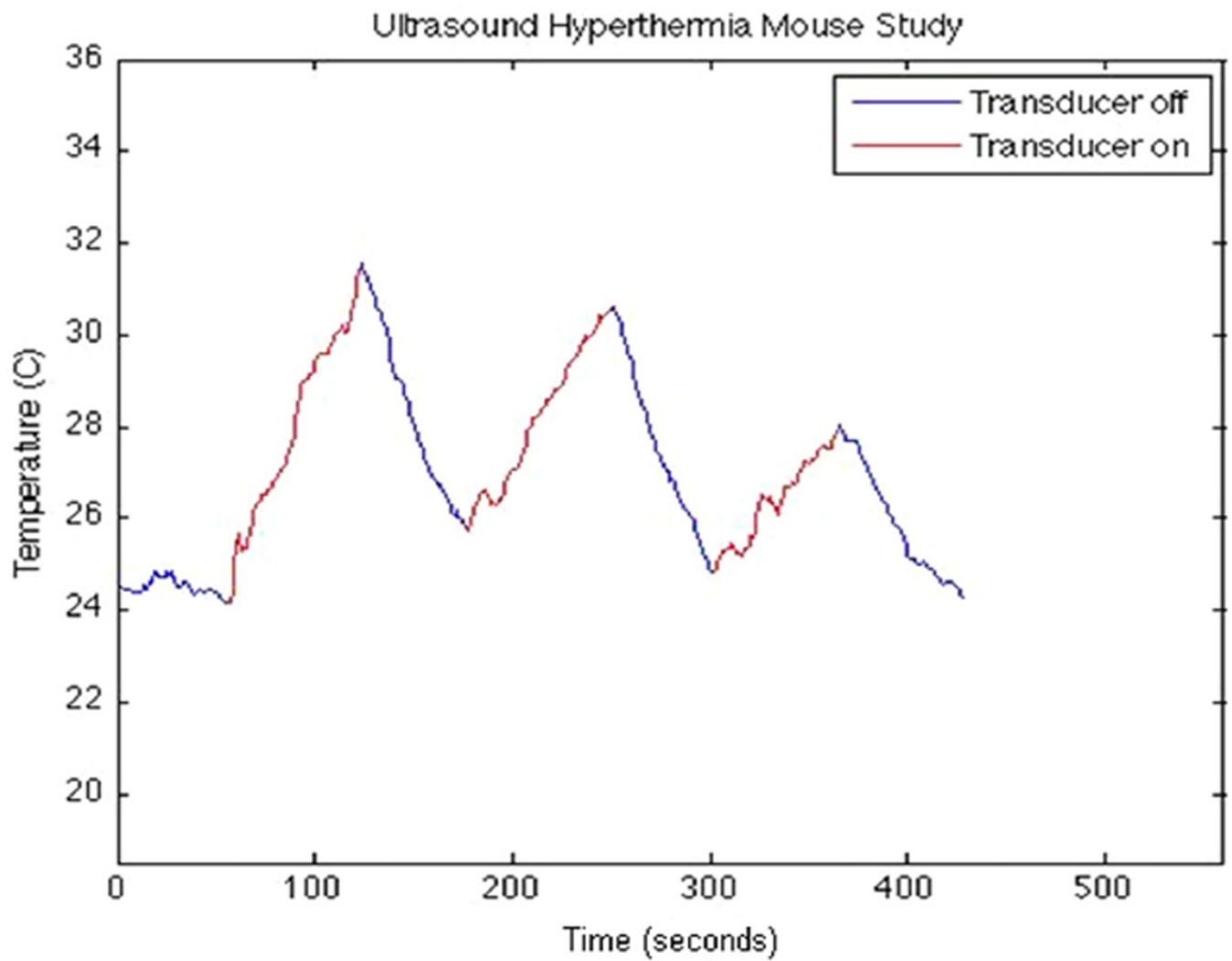
Figure 7.
Apparatus for heating human glioblastoma xenograft with thermocouple (black arrow) 2 mm
deep. Transducer (red arrow) placed above center of thermocouple needle.
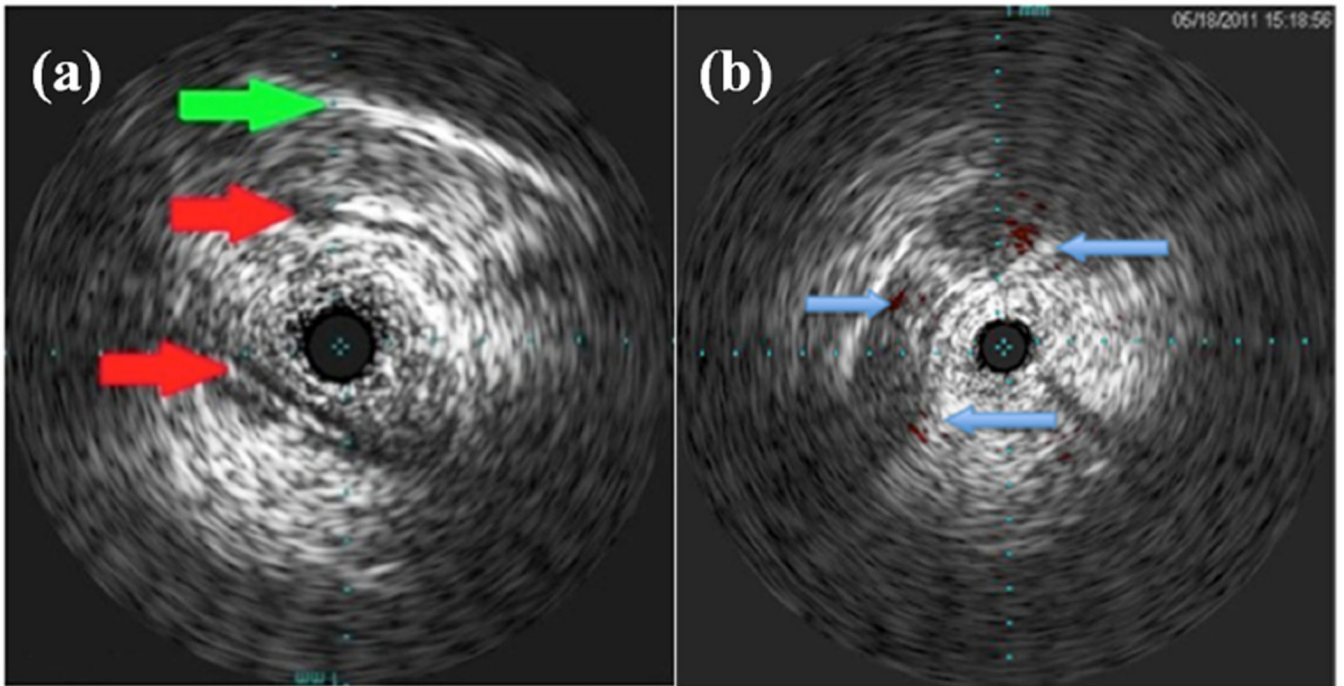
Figure 8.
In vivo porcine brain 20-MHz images for unmodified transducer. (a) Distinguished blood vasculature (red arrows) and skull (green arrow). (b) Coronal view of porcine brain with arrows indicating cross-section of blood vessels with Volcano ChromaFlo. Tick marks show 1-mm spacing.

Figure 9.
Heating graphs. Top: 8.5°C temperature increase of tissue phantom for 60 seconds of heating. Bottom: 2°C temperature increase of backside of transducer in the same trial.

Ultrasound Hyperthermia Mouse Study

Figure 10.
Xenograft from thermocouple data showing sequential temperature rises of 8°C, 4.5°C, and 3°C after 90 seconds of heating for electric power levels of 2.2 W, 1.2 W, and 900 mW, respectively.
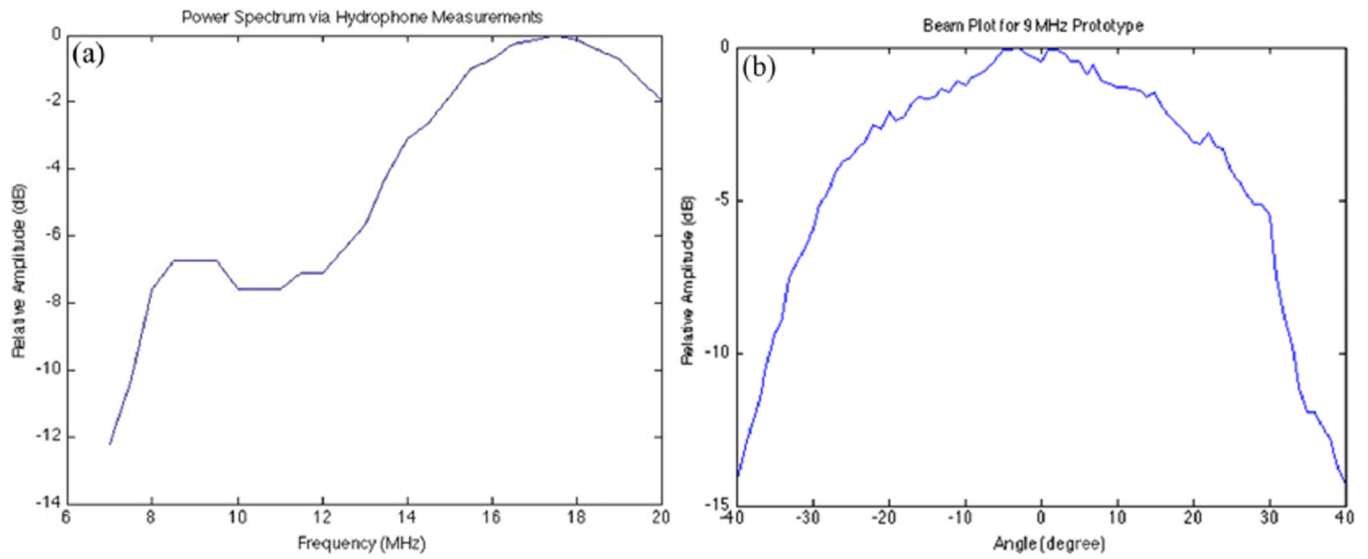
Figure 11.
(a) Power spectrum found by sweeping a 60-V, three-cycle sine wave excitation from 7 MHz to 20 MHz. (b) Beam plot for 9-MHz transducer prototype with a −6-dB width of roughly 63 degrees.
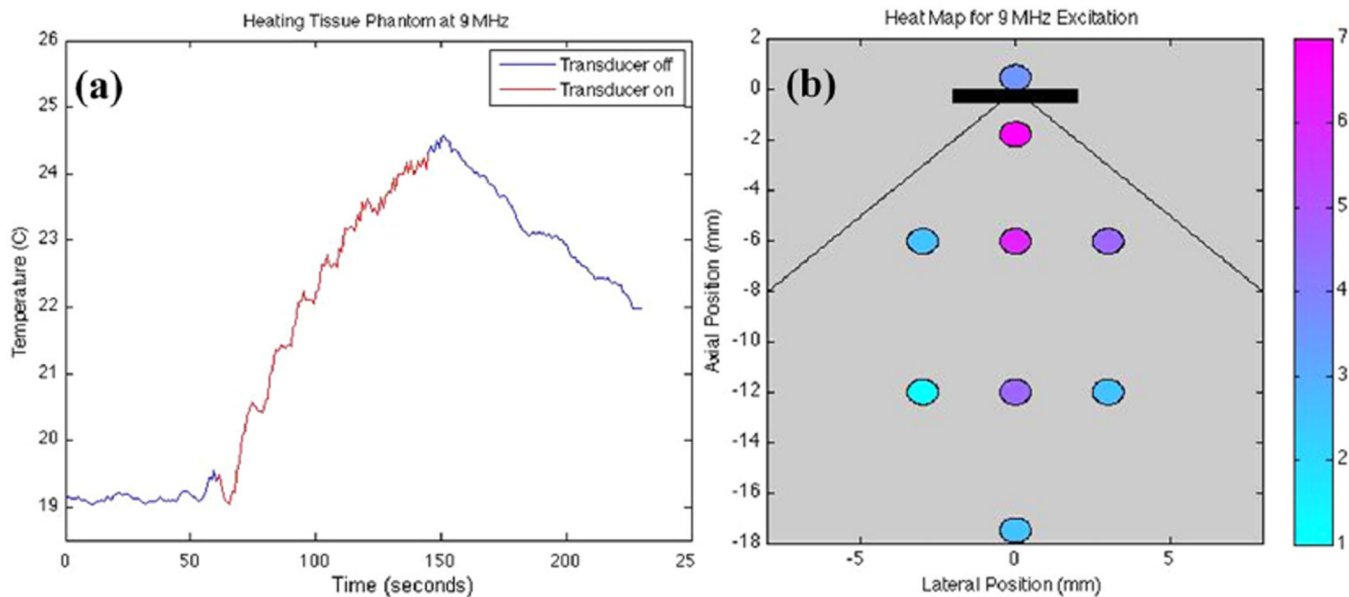
Figure 12.
(a) Thermocouple data for 60 seconds of heating at 9 MHz. ISPTP of 2.56 W/cm^2 leads to a 5.5°C temperature rise. (b) Heating map in tissue phantom. Each data point corresponds to the maximum temperature rise after 90 seconds of 9-MHz excitation with ISPTP of 2.56 W/cm^2. The black rectangle represents the transducer with the extended lines showing the ideal beam width of 90 degrees. Net forward electric power was 2.8 W.